World Journal of Advanced Engineering Technology and Sciences
eISSN: 2582-8266
Cross Ref DOI: 10.30574/wjaets
Journal homepage: https://wjaets.com/

(RESEARCH ARTICLE)

Check for updates

A systematic robust polytopic framework for control co-design

Stefany Patricia Dutra and Alexandro Garro Brito *

Federal University of Santa Catarina – UFSC, R. Dona Francisca 8300, CEP: 89219-600. Joinville/SC – Brazil.

World Journal of Advanced Engineering Technology and Sciences, 2026, 18(02), 131-147

Publication history: Received on 01 January 2026; revised on 07 February 2026; accepted on 10 February 2026

Article DOI: https://doi.org/10.30574/wjaets.2026.18.2.0086

Abstract

Contemporary technological systems increasingly require integrated plant and controller design to ensure robust closed-loop performance. Control co-design addresses this challenge by simultaneously optimizing plant and controller parameters within a unified framework. This article proposes a robust control co-design methodology based on polytopic H∞ optimization for linear systems. The approach employs a two-level optimization strategy that guarantees closed-loop stability throughout the entire design process, from plant parameter selection to controller synthesis. The proposed framework provides a systematic and reusable reference for robust co-design problems subject to parametric uncertainty. The effectiveness of the method is demonstrated through an automotive active suspension system, where the proposed approach achieves improved closed-loop performance compared to conventional sequential plant-controller design strategies.

Keywords: Robust Control; LMI; Control Co-Design; Automotive Active Suspension.

1. Introduction

The conventional design of practical systems is based on searching for the parameters of the mechanical structure, followed by the control design, in order to improve the overall performance of the system [1]. The main disadvantage of solving these two problems sequentially is that it does not guarantee global optimization of the dynamic system [2]. Therefore, the conventional method does not guarantee the ideal coupling between the mechanical design and the control system, producing suboptimal results [3].

Design strategies that manage the coupling between the artifact and the control system are known as control co-design. These approaches aim to carry out the project based on the balance between the performance of the mechanical structure and the controller. In this manner, an integrated method for obtaining both plant and controller parameters allows the achievement of an optimal system design [1].

Several optimization strategies can be applied to the control co-design problems [4]. Among them are sequential, iterative, nested, and simultaneous optimization procedures. Because of the improved performance provided by control co-design, this area has been the subject of intense research [5]. Recent studies include automotive systems [3, 6–12], modern renewable energy systems [13–15], thermal management systems [16], and spacecraft systems [17]. In addition, the application of co-design approaches to deterministic and uncertain problems has also been investigated [18], as well as nonlinear problems [19].

Recent literature has presented several results on robust control applied to control co-design problems. In [20], a comprehensive review of control co-design of uncertain systems is provided. In [21], a co-design algorithm based on robust model predictive control (MPC) is discussed. The idea was to use the MPC algorithm as the inner loop of the control co-design. According to the authors, this strategy can guarantee the feasibility of the MPC optimization when the

* Corresponding author: Alexandro Garro Brito.

co-design problem is formulated with bounded additive uncertainties. Another predictive methodology based on a tube-based MPC algorithm is discussed in [22]. One of the main features is to provide performance-robustness trade-offs through Pareto fronts. Robust control co-design involving set-based methodologies was proposed in [23]. The technique provides the reachability analysis for closed-loop safety for uncertainties and exogenous inputs.

There is a vast literature concerning the application of *Linear Matrix Inequalities (LMIs)* in control systems. Due to recent improvements in algorithms for convex optimization, many important control problems can now be solved efficiently [24, 25]. Significant solvers and parsers have been developed to address the computation of LMI problems [26, 27]. In the context of robust control, H_2 and H_∞ controller designs take advantage of LMI convex optimization, since plant uncertainties exhibit certain properties [28]. Among the recent results in LMI control, we can cite adaptive control [29, 30], robust fault-tolerant control [31], and learning control [32].

In this work a Robust Polytopic Optimization strategy, referred to as "*RPO*" herein, is proposed to solve control co-design problems of linear systems through a combined plant and robust controller optimization. The controller optimization is based on a LMI H_∞ design that considers the dispersion of the plant parameters in a polytopic framework. Once the optimal controller is found, it is applied to the plant optimization procedure. As the calculated controller is suboptimal, and it ensures stability for any plant inside such polytope (including the optimal one), a new smaller polytope is created around the optimal parameters of the plant. Then, the procedure is repeated until the co-design solution is found. The main idea behind the method is to construct a two-part interactive optimization where: *i)* the plant is optimized inside a parameter polytope for which there is a robust stabilizing controller, and; *ii)* the polytope is progressively reduced around the optimal plant solution, to reduce the controller conservativeness.

The proposed technique has some important features. Firstly, the plant-controller optimization guarantees closed-loop stability at every algorithm step. Optimization solvability significantly benefits when plant uncertainties are formulated in a polytopic format, thanks to the extensive studies and proven algorithms already available. In addition, technical difficulties are avoided when a nested plant-controller optimization is adopted, in comparison to simultaneous control co-design methods [33–37].

As a case study, the RPO method is used for the co-design of an automotive active suspension. The system spring and damper are used as the plant parameters to be optimized. On the other hand, the H_∞ controller is applied to guarantee that the active suspension achieves safety and comfort requirements for the passengers.

The remainder of the paper is organized as follows. Sec. 2 presents an overview of the four co-design strategies. Sec. 3 reviews the LMI H_∞ robust control. Sec. 4 describes the algorithm of the co-design through robust control. Sec. 5 discusses the usage of the strategy on a case study of a vehicle active suspension. Sec. 6 illustrates the efficacy of the proposed algorithm when applied to the active suspension system. Finally, Sec. 7 presents the conclusions.

2. Optimization strategies

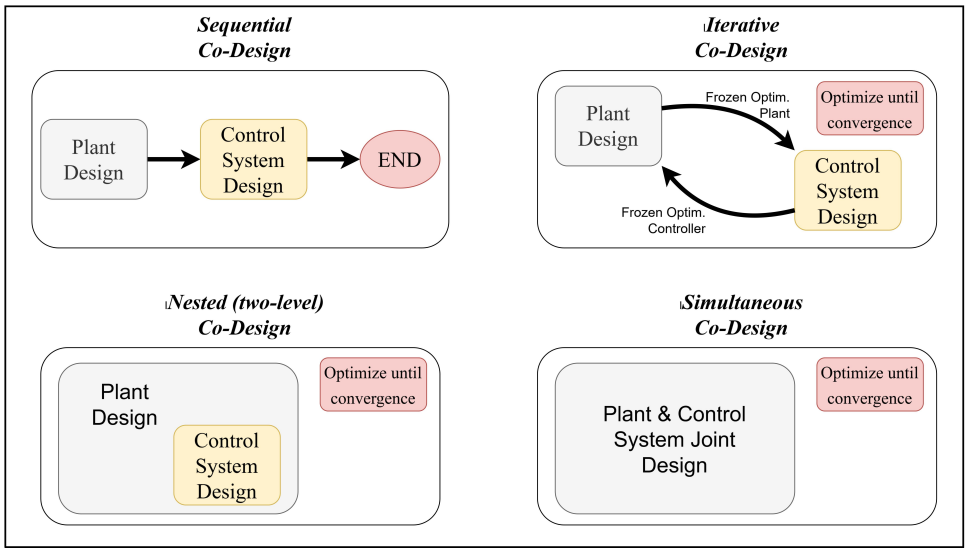

Figure 1 Co-Design optimization strategies.

Studies on control co-design can be found in different contexts in the literature. The main strategies can be divided into four categories [4]: sequential, iterative, nested, and simultaneous, as illustrated in Figure 1.

The sequential strategy is the conventional approach for solving the plant-controller design. In this case, there are two separate optimization problems. The plant is first optimized, followed by the controller design. If there are any couplings between these problems, the controller is completely ignored during the plant optimization. If certain controller parameters are necessary in plant optimization, they are assigned assumed (fixed) values. Once the optimal plant is obtained, the controller design is performed. Although simpler to solve, the sequential strategy can achieve the global optimum for the plant-controller system only if the two problems are completely uncoupled. Depending on the nature of the coupling, the method can fail to provide an optimal solution for the controller, or even for the overall system [4, 38, 39].

In the iterative strategy, the co-design problem is iteratively solved. The artifact design is first performed by assuming an initial controller. Next, the controller design is performed with the artifact parameters held constant. This controller is then applied to a new plant optimization. In this approach, the solution of each iteration becomes the starting point of the new iteration. This cycle is repeated until convergence criteria are met. The main advantage of this strategy is that the two optimization problems maintain a separate structure. However, convergence cannot be guaranteed for all cases, nor can convergence to a globally optimal solution [4, 39].

The nested (or two-level) optimization strategy requires two optimization routines: an outer loop that solves the optimal artifact design problem, and an inner optimization loop that identifies the optimal controller for each artifact design considered by the outer loop [38]. In the nested approach, the plant design evaluated in the outer loop is used to determine the next iteration, for example, by determining derivatives and taking an optimization step. The main advantage of the nested approach is the ability to employ existing control design methods to solve the inner loop problem, without the complexity of managing artifact design variables [38].

The simultaneous co-design optimizes artifact and control variables in the same optimization formulation. That is, the simultaneous optimization algorithm attempts to optimize a combined artifact-controller objective function by varying the artifact and controller designs simultaneously, subject to the combined set of artifact and controller constraints [38]. This approach has the advantage that, if a solution is found, the resulting system is optimal. The main issue of this strategy refers to the design complexity, since the optimization problem cannot be solved until the artifact and control objectives have been formulated. This requires that the control architecture should be decided early in the design process [39].

3. LMI H_∞ Robust Control

The application of the LMI H_∞ robust control to polytopic uncertain systems has been well established in the literature. Hence, only the main concepts are presented herein, following the discussions in [40, 41].

Consider a control system with the configuration shown in Figure 2. In this paper, a static-state feedback is assumed, with $P(s)$ and K representing the plant and the controller respectively. The signals u and w are, respectively, the control input and disturbance input. The signals y and z are, respectively, the sensed output and the disturbance rejection output. In addition, x represents the state variables of the plant.

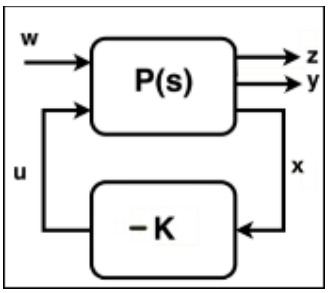

Figure 2 Block diagram of a robust control closed loop.

Assume a plant $P(s)$ with uncertainties on the parameters given by Eq. (1):

$$P(s) \triangleq \begin{cases} \dot{\vec{x}}(t) = \boldsymbol{A}(\vec{\xi})\vec{x}(t) + \boldsymbol{B_1}(\vec{\xi})w(t) + \boldsymbol{B_2}(\vec{\xi})u(t) \\ z(t) = \boldsymbol{C_1}(\vec{\xi})\vec{x} + \boldsymbol{D_{11}}(\vec{\xi})w(t) + \boldsymbol{D_{12}}(\vec{\xi})u(t) \\ y(t) = \boldsymbol{C_2}(\vec{\xi})\vec{x}(t) + \boldsymbol{D_{21}}(\vec{\xi})w(t) + \boldsymbol{D_{22}}(\vec{\xi})u(t) \end{cases} \tag{1}$$

This paper considers a static-state feedback controller $u(t) = -Kx(t)$. Therefore, the closed-loop system from $w(t)$ to $z(t)$ is given by Eq. (2):

$$\begin{cases} \dot{\vec{x}}_{cl} = \tilde{\boldsymbol{A}}(\vec{\xi})\vec{x}_{cl}(t) + \tilde{\boldsymbol{B}}(\vec{\xi})w(t) \\ z(t) = \tilde{\boldsymbol{C}}_{\boldsymbol{z}}(\vec{\xi})\vec{x}_{cl}(t) + \tilde{\boldsymbol{D}}_{\boldsymbol{z}}(\vec{\xi})w(t) \\ y(t) = \tilde{\boldsymbol{C}}_{\boldsymbol{y}}(\vec{\xi})\vec{x}_{cl}(t) + \tilde{\boldsymbol{D}}_{\boldsymbol{y}}(\vec{\xi})w(t) \end{cases} \tag{2}$$

with: $\boldsymbol{A}^{\sim} = \boldsymbol{A} - \boldsymbol{B_2K}$; $\boldsymbol{B}^{\sim} = \boldsymbol{B_1}$; $\boldsymbol{C}^{\sim}_{\boldsymbol{z}} = \boldsymbol{C_1} - \boldsymbol{D_{12}K}$; $\boldsymbol{C}^{\sim}_{\boldsymbol{y}} = \boldsymbol{C_2} - \boldsymbol{D_{22}K}$; $\boldsymbol{D}^{\sim}_{\boldsymbol{z}} = \boldsymbol{D_{11}}$, and; $\boldsymbol{D}^{\sim}_{\boldsymbol{y}} = \boldsymbol{D_{21}}$ (where the parameter dependence on the matrices was dropped for brevity). In this case, the closed loop transfer function from $w(t)$ to $z(t)$ is given by $T_{wz}(s) = \boldsymbol{D}^{\sim}_{\boldsymbol{z}} + \boldsymbol{C}^{\sim}_{\boldsymbol{z}}(\boldsymbol{sI} - \boldsymbol{A}^{\sim})^{-1}\boldsymbol{B}^{\sim}$. The infinity norm of this transfer function is defined as $||Twz(s)||_\infty \triangleq sup_\omega\ |Twz(j\omega)|$.

Let a *unity simplex* be written as

$$\mathcal{U} = \left\{ \vec{\xi} \in \mathbb{R}^N \ : \ \sum_{i=1}^{N} \xi_i = 1,\ \xi_i \geq 0,\ i = 1, \cdots, N \right\}. \tag{3}$$

Furthermore, consider that each state matrix can be written as a convex combination of *N* matrices:

$$\boldsymbol{\mathcal{P}} \triangleq \left(\boldsymbol{A}(\vec{\xi}), \boldsymbol{B_1}(\vec{\xi}), \cdots, \boldsymbol{D_{22}}(\vec{\xi}) \right) = \sum_{i=1}^{N} \xi_i \left(\boldsymbol{A_i}, \boldsymbol{B_{1,i}}, \cdots, \boldsymbol{D_{22,i}} \right), \tag{4}$$

with $\xi \in U$, and *N* being the number of uncertain parameters. Such uncertain model is then referred to as a *polytopic* system. Hence, the closed loop matrices in Eq. (2) can also be written in a polytopic framework, resulting in:

$$\boldsymbol{\mathcal{P}_{cl}} \triangleq \left(\tilde{\boldsymbol{A}}(\vec{\xi}), \tilde{\boldsymbol{B}}(\vec{\xi}), \cdots, \tilde{\boldsymbol{D}}_{\boldsymbol{y}}(\vec{\xi}) \right) = \sum_{i=1}^{N} \xi_i \left(\tilde{\boldsymbol{A}}_{\boldsymbol{i}}, \tilde{\boldsymbol{B}}_{\boldsymbol{i}}, \cdots, \tilde{\boldsymbol{D}}_{\boldsymbol{y,i}} \right), \tag{5}$$

The H_∞ *control* consists of designing a controller such that the closed loop is stable for any plant model contained within the polytope, and the infinity norm of the transfer function $T_{wz}(s)$ is suboptimal. This problem can be solved through the well-known bounded real lemma as follows.

Lemma (Bounded Real [24]) Consider the closed-loop system as in Eq. (2), with polytopic uncertainties described in Eq. (4). The following statements are equivalent:

(i) the closed loop system is stable;

(ii) $||Twz(s)||_\infty < \gamma \in \mathbb{R}$;

(iii) there exists a symmetric positive definite solution *P* to the LMI

$$\boldsymbol{\mathcal{S}}_i = \begin{bmatrix} \tilde{\boldsymbol{A}}_{\boldsymbol{i}}\boldsymbol{P} + \boldsymbol{P}\tilde{\boldsymbol{A}}_{\boldsymbol{i}} & \boldsymbol{P}\tilde{\boldsymbol{B}}_{\boldsymbol{i}} & \tilde{\boldsymbol{C}}_{\boldsymbol{i}}^{\ T} \\ \star & -\gamma\boldsymbol{I} & \tilde{\boldsymbol{D}}_{\boldsymbol{z,i}} \\ \star & \star & -\boldsymbol{I} \end{bmatrix} < 0, \tag{6}$$

with $i = 1, \dots, N$.

(iv) there exists matrices $\boldsymbol{Q} = \boldsymbol{Q^T} > 0, \boldsymbol{Q} = \boldsymbol{P}^{-1}$ and $\boldsymbol{W} = \boldsymbol{KQ}$ that are the solutions to the LMI's:

$$\begin{bmatrix} \boldsymbol{QA_i}^T + \boldsymbol{A_iQ} - \boldsymbol{B_{2i}W} - \boldsymbol{W}^T\boldsymbol{B_{2i}} & \boldsymbol{B_{1i}} & \boldsymbol{QC_i}^T - \boldsymbol{W}^T\boldsymbol{D_{12i}}^T \\ \star & -\gamma\boldsymbol{I} & \boldsymbol{D_{11i}}^T \\ \star & \star & -\boldsymbol{I} \end{bmatrix} < 0, \tag{7}$$

with $i = 1, \dots, N$.

Eq. (7) presents the LMI's as a function of the plant matrices. This is used for direct computation of the controller in a linear framework. Such an equation is obtained by the congruence transformation $\boldsymbol{L^T S_i L}$, with $\boldsymbol{L} = diag(\boldsymbol{P}^{-1}, \boldsymbol{I}, \boldsymbol{I})$, and "*diag*" denoting a block diagonal matrix.

The controller design for polytopic uncertain plants is quite conservative for fixed Lyapunov matrix $\boldsymbol{P}$. Some results are presented in the literature to reduce such conservativeness by using parametrized Lyapunov matrices (e.g. [28]). However, the fixed Lyapunov matrix is still assumed in this paper, since the polytopic set size is progressively reduced along the co-design optimization procedure (see Section IV).

3.1. Control Co-Design Through Robust Polytopic Optimization – RPO

In general, the plant–controller co-design can be described by

$$\begin{aligned} \min_{\vec{x}_p, \vec{x}_c} \quad & f(\vec{x}_p, \vec{x}_c, t) \\ \text{s.t.} \quad & h(\vec{x}_p, \vec{x}_c, t) = 0 \\ & g(\vec{x}_p, \vec{x}_c, t) \leq 0 \end{aligned} \tag{8}$$

where f is the objective function to be minimized, $\vec{x}_p$ and $\vec{x}_c$ are, respectively, the design parameter vectors of the plant and controller to be determined, h and g are the equality and inequality constraints, respectively. In a typical control co-design problem, the objective function can be split so that

$$f(\vec{x}_p, \vec{x}_c, t) = f_p(\vec{x}_p, \vec{x}_c, t) + f_c(\vec{x}_p, \vec{x}_c, t), \tag{9}$$

where f_p and f_c represent objective functions for the plant and the controller, respectively.

The paper proposes an approach to perform the control co-design optimization for systems, which can be cast in a polytopic modeling framework. Herein, such methodology is referred to as *Robust Polytopic Optimization – RPO*. The method is schematically presented in Figure 3, where each algorithm block is explained as follows:

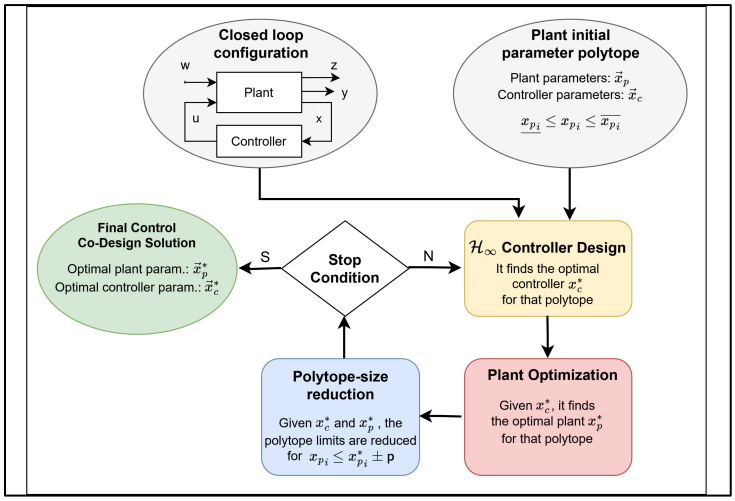

Figure 3 Control co-design through Robust Polytopic Optimization (RPO): schematic illustration of the methodology.

- **Closed loop configuration**: This action is related to the controller and closed-loop framework adopted during the control co-design. It follows the concepts presented in the Section III;
- **Initial polytopic model**: Firstly, each of the plant design parameters in $\vec{x}_p$ are limited by a range with extreme values *(min(x_{pi}) ≤ x_{pi} ≤ max(x_{pi}))*. This range takes into account, for example, physical and constructive restrictions for that given plant parameter. The plant is then modeled as a linear uncertain polytopic system, as presented in Eqs. (1) and (4);
- H_∞ **controller design**: In this step, a polytopic H_∞ control design is performed. The initial polytope – based on the nominal parameters and their constructive limitations – is used in the first algorithm iteration. For the other co-design iterations, the reduced-size polytope is used (see the step "polytope-size reduction" below). Basically, the controller design follows the convex optimization of Eq. (7), which results in a state-feedback matrix ***K***. It is important to observe that the Lyapunov matrix ***P*** (and also ***W*** and ***Q*** in Eq. (7)) is not kept fixed throughout the control co-design procedure. This implies that new Lyapunov matrices are computed for each H_∞ controller design. Such a procedure aims to reduce controller conservativeness along the polytope-size management, by searching a new suboptimal controller for each new reduced polytope.
- **Plant optimization**: Once a stabilizing controller is obtained, the plant can then be optimized within the polytope range. Notice that we are interested in obtaining optimized plant parameters x_{pi} that minimize a certain objective function $f(\vec{x}_p, \vec{x}_c, t)$ with the controller kept frozen from the last step. This implies that the optimization is performed in a closed-loop sense, i.e. the plant that achieves the minimum cost function level for that closed loop configuration. Because of this, $f(\vec{x}_p, \vec{x}_c, t)$ should measure the overall system performance.
- This step is only possible due to the methodology proposed in this paper. As the controller is stabilizing for any plant inside the polytope, it will also be stabilizing for the optimal plant. If this strategy is not applied, the plant optimization could interfere with the closed loop stability with a frozen controller, and the optimization consistency could be lost.
- **Polytope-size reduction:** A known issue in robust control is the conservativeness. The fact of obtaining a stabilizing controller for a wide set of plants (expressed by the polytope) provides a suboptimal solution that is obviously conservative. A strategy to circumvent such issue is to use parameter-dependent Lyapunov matrices along the convex optimization of the LMIs in Eq. (7). There are presently proper parsers to solve that problem [27].

This paper adopts an alternative way to reduce the conservativeness during the co-design optimization. By taking the optimal plant parameters $x^*_{p,i}$ from the last plant optimization, a new polytope is created around this solution. This new reduced polytope is used for the robust controller design. After this, the plant optimization is again performed by keeping the controller frozen along this optimization. With the new optimal plant of this stage, a new reduced polytope can be obtained. The procedure is then repeated until the stopping condition of the co-design process. Figure 4 illustrates the procedure of polytope reduction.

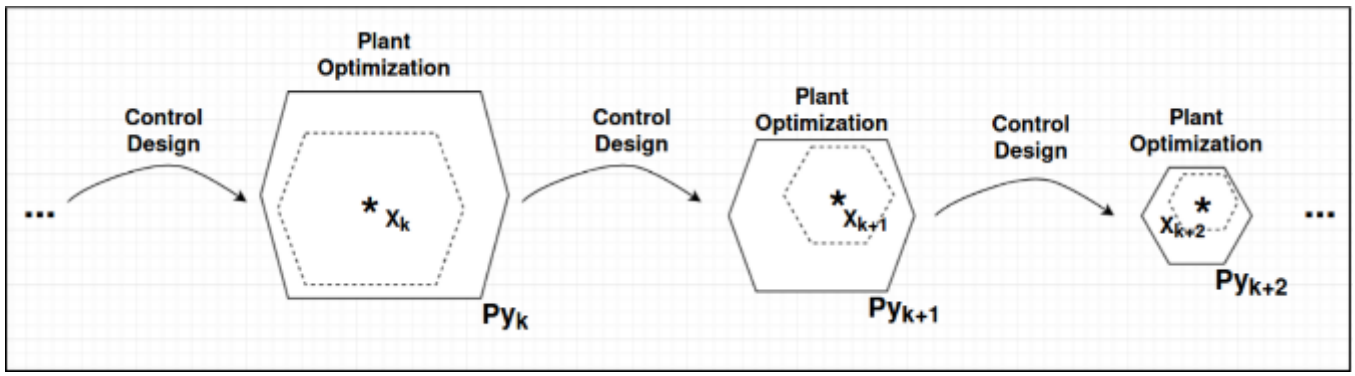

Figure 4 Polytope-size reduction. Py_j denotes the polytope used in the robust controller design (continuous line), while x_j represents the optimal plant solution for that polytope. Once an optimal plant solution is found, a new polytope is created around it (dashed line). The controller-plant optimization is then repeated for this reduced polytope. This methodology progressively reduces the controller's conservativeness throughout the co-design procedure

A strategy for a systematic polytope-size reduction along the co-design procedure is taking a percentage *p* of each optimized plant parameter, which is progressively reduced along the plant-controller co-design optimization. The choice of the percentage p is obviously related to the practical co-design problem in discussion. However, a drastic

polytope-size reduction should be avoided along the iterations, because this can jeopardize the optimization evolution along the process (e.g. loss of the optimal solution);

- **Stopping condition:** At this stage, some iterative stopping condition should be tested. As an example, one could test the present polytope size: if it is small enough, this means that we are close to the problem optimum. An alternative would be to limit the minimum amount of variation of the optimal cost-function. Once the stopping condition is achieved, the optimal pair plant-controller is obtained.

Some remarks about the methodology are addressed as follows. By writing the uncertain plant in the polytopic format, one can ensure convexity during the controller optimization – an important feature. Moreover, the H_∞ design provides closed-loop stability for any plant inside the polytope, and this condition is not lost during the plant optimization. As the polytope size is reduced along the iterations, the controller tends to become less conservative.

In many aspects, the proposed co-design approach blends characteristics of the iterative and nested co-design strategies. However, it is important to notice that the features previously discussed cannot always be achieved by many iterative and nested co-design methodologies when an ordinary optimization method is applied [12].

4. Case Study: Vehicle Active Suspension

Demands for better ride comfort, vehicle handling, and safety have motivated many automotive manufacturers to consider the use of active suspensions [42]. Active suspensions, capable not only of storing and dissipating energy but also of introducing it into the system, can better resolve the trade-off among these conflicting performance requirements [8]. In this article, the co-design of a quarter-car active suspension aims to improve the system's performance in terms of driving comfort and vehicle safety.

The dynamics of the suspension are based on the quarter-car model, represented by a linear system of two degrees of freedom, as shown in Figure 5. In this model, the sprung mass m_s represents a quarter of the total body mass of the vehicle, and the unsprung mass m_u represents the axle-wheel assembly. The suspension system consists of a spring with elastic constant k_s in parallel with a shock absorber with damping coefficient b_s. The active control force $F_A(t)$ is applied between the two masses by means of an

actuator. The elastic constant of the tire is called k_t. The two degrees of freedom of the model are represented by the vertical displacement of the sprung mass $Z_s(t)$, and vertical displacement of the mass unsprung $Z_u(t)$. The disturbance $Z_r(t)$ is caused by the road surface irregularities.

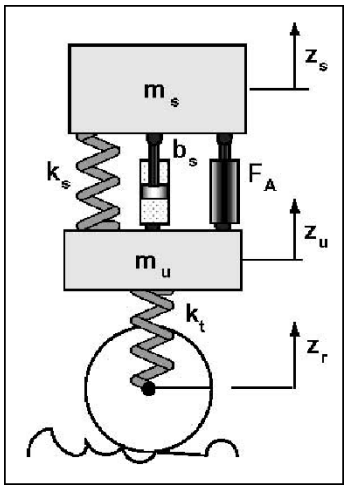

Figure 5. Quarter-car vehicle suspension model [43].

The dynamic model of the system can be described by

$$\dot{\vec{x}}(t) = \boldsymbol{A}\vec{x}(t) + \boldsymbol{B_A}F_A(t) + \boldsymbol{B_r}Z_r(t) \tag{10}$$

where $\vec{x}(t)$ is the state vector, defined by

$$\begin{bmatrix} x_1(t) \\ x_2(t) \\ x_3(t) \\ x_4(t) \end{bmatrix} = \begin{bmatrix} Z_s(t) - Z_u(t) \\ \dot{Z}_s(t) - \dot{Z}_u(t) \\ Z_u(t) \\ \dot{Z}_u(t) \end{bmatrix} \tag{11}$$

where $x_1(t)$ the vertical displacement between sprung mass and unsprung mass, $x_2(t)$ the velocity between sprung mass and unsprung mass, $x_3(t)$ the vertical displacement of the unsprung mass and $x_4(t)$ the velocity of the unsprung mass. The matrices A, B_A and B_r are given by

$$\boldsymbol{A} = \begin{bmatrix} 0 & 1 & 0 & 0 \\ -k_s\left(\frac{1}{m_s} + \frac{1}{m_u}\right) & -b_s\left(\frac{1}{m_s} + \frac{1}{m_u}\right) & \frac{k_t}{m_u} & 0 \\ 0 & 0 & 0 & 1 \\ \frac{k_s}{m_u} & \frac{b_s}{m_u} & \frac{k_t}{m_u} & 0 \end{bmatrix}; \tag{12}$$

$$\boldsymbol{B_A} = \begin{bmatrix} 0, & \left(\frac{1}{m_s} + \frac{1}{m_u}\right), & 0, & \frac{-1}{m_u} \end{bmatrix}^T; \tag{13}$$

$$\boldsymbol{B_r} = \begin{bmatrix} 0, & -\frac{k_t}{m_u}, & 0, & \frac{k_t}{m_u} \end{bmatrix}^T. \tag{14}$$

The parameters k_s and b_s have been treated as independent design variables in many co-design works, but it is known that, in fact, they depend on geometric design and constraints. Here, based on the study in [3], k_s and b_s are treated as dependent variables through geometric constraints. Herein, it is used a plant model that calculates the spring and damper coefficients as a function of their independent geometric variables.

4.1. Spring design

Figure 6 illustrates a helical compression spring with square and ground ends. The coil spring surrounds the damper, and they are coaxial.

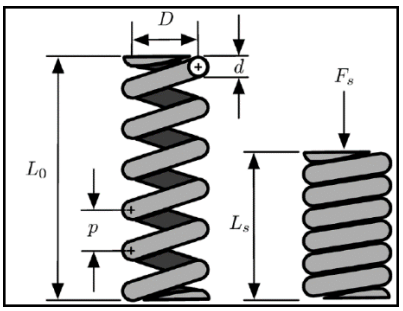

Figure 6 Helical compression spring with squared ground ends [3].

The free length of the spring is $L_o = pN_a + 2d$ and the solid height is $L_s = d(N_a + 3)$, where p is the spring pitch and N_a is the number of active coils. The spring constant is:

$$k_s = \frac{d^4 G}{8D^3 N_a \left(1 + {}^1\!/_{2C^2}\right)} \tag{15}$$

where d is the wire diameter, G is the shear modulus, D is the helix diameter and C is the spring index [44].

4.2. Damper design

In the project, a single-tube telescopic damper is considered where linear damping is assumed. The damper's working principle, its damping and thermal properties can be found in [3]. The damper coefficient is:

$$b_s = \frac{D_p^4}{8C_d\eta A_f\sqrt{x_m}D_o^2}\sqrt{\frac{\pi k_v \rho_1}{2}} \tag{16}$$

where k_v is the spool valve spring constant, ρ_1 is the damper fluid density, C_d is the discharge coefficient and D_o is the valve diameter. The coefficient η defines the upper limit of the proportion of the external circumference of the spool valve that can be exposed. The area factor A_f is used to adjust the shape of the door and x_m is the maximum elevation of the valve at the maximum pressure allowed in the damper, given by:

$$x_m = \frac{D_o^2 b_s V_{max}}{D_p^2 k_v} \tag{17}$$

where V_{max} is the maximum piston speed of the shock damper.

4.3. Project geometric constraints

The construction of the spring and the damper is subjected to several geometric constraints. The spring index C is limited to a range between 4 and 12 for commercial automotive applications. The spring free length should be limited to a maximum available space L_{omax}. The internal and external spring diameters should be constrained to extreme values D_{intmin} and D_{extmax}, respectively. In addition, the spring internal diameter should be larger than the damper diameter, by a specified clearance. Additional constraints related to the spring and damper materials can also be included [3]. All these design constraints enter into the system optimization, and they should be taken into account during the co-design procedure.

4.4. Control co-design optimization

The plant design vector $\vec{x}_p$ is composed of the helix diameter D, the wire diameter d, the spring pitch p, the damper piston diameter D_p and the valve diameter D_o. These parameters are subjected to the physical constraints already mentioned. The variable $\vec{x}_c$ represents the design parameters of the controller to be determined during the optimization process. Herein, we aim at the complete design of the spring and the damper artifacts, as well as the optimum controller.

Some co-design objectives were established in this paper, as follows. Firstly, the design aims at the disturbance minimization due to track irregularities. This takes into account three important features to be provided by an active suspension: *i)* the passenger comfort, measured through the amount of vertical car acceleration; *ii)* the vehicle safety, ensuring proper levels of the contact force between the tire and the track, and; *iii)* the component life cycle, by minimizing the vertical displacement of the suspension rod. These three criteria can be formulated within a robust control framework, in which one obtains an optimal controller that minimizes the H_∞ norm from the road disturbance input (Z_r) to the affected variables ($\ddot{Z}_s$, $Z_u - Z_r$ and $Z_s - Zu$ respectively).

Another important design objective is the weight reduction of the suspension system. This can be accomplished by the minimization of the spring weight φ. A detailed analysis of the mechanical parameters involved in such weight minimization is available in the literature [44].

The absolute maximum shear stress on the walls of the shock absorber body – τ – must be minimized in order to increase its useful life. This is another plant objective that should be used during the optimization [45].

Then, the co-design problem can be formulated as a weighted optimization of these three requirements as follows:

$$J_{plant} = w_1\frac{\mathcal{H}_\infty}{\mathcal{H}_{\infty,max}} + w_2\frac{\varphi}{\varphi_{max}} + w_3\frac{\tau}{\tau_{max}} \tag{18}$$

where the maximum acceptable values are considered for the robust norm ($H_{\infty,max}$), for the spring weight (φ_{max}) and for the absolute shear stress (τ_{max}). These weights w_1, w_2, and w_3 can be chosen to reinforce the relative importance among the optimization criteria.

5. Simulation Results

The nominal suspension data were taken from [46], referring to a 2006 Fiat Uno vehicle, with its parameters defined in Table 1. The optimization parameters consist of the helix diameter D [m], the wire diameter d [m], the spring pitch p [m], the damper piston diameter D_p [m], and the valve diameter D_o [m]. The nominal values of the helix diameter, the

wire diameter and the number of active coils for the spring consist respectively of D = 0.123 m, d = 0.012 m and N_a = 6. Specifying the free length of the spring L_{omax} = 0.330 m and using $L_o - L_{omax} \leq 0$, with the nominal values of d and N_a, we obtain p = 0.051 m.

Table 1 Parameters referring to a quarter of a Fiat Uno car.

Variable	Description	Value
m_s	Sprung mass	260 kg
m_u	Unsprung mass	31.5 kg
k_s	Suspension spring stiffness coefficient	16878.32 N/m
b_s	Suspension damper damping coefficient	1554 N.s/m
k_t	Tire stiffness coefficient	190000 N/m

The upper and lower limits of the helix diameter are defined as being 30% of the nominal value and the wire diameter as being 25% of the nominal value. The minimum internal diameter is defined as being $D_{int,min}$ = 0.071 m and the maximum external diameter as being $D_{ext,max}$ = 0.175 m. The spring design considers ASTM A401 steel, which has a modulus of elasticity of E = 203.4 GPa and a shear modulus of G = 77.2 GPa. According to [3], a gap of δ_{dc} = 0.0090 m between the spring and the damper, and the shock absorber wall thickness is t_d = 0.0020 m.

In the design of the damper, the discharge coefficient is specified as being approximately C_d = 0.70 for spool valves. The spool valve spring constant is k_v = 7500 N/m, and the fluid density of the damper is ρ_1 = 850 kg/m^3. Consider η = 0.9 and A_f = 0.1 [3].

The nominal value of the piston diameter was estimated based on the literature, which informs that, for a McPherson-type automotive front suspension, the value of the piston diameter can be 0.030 m or 0.032 m [47]. We considered D_p = 0.030 m as the lower limit, and D_p = 0.036 m as the upper limit. The lower and upper bounds of the valve diameter are 0.0042 m and 0.0061 m, respectively. Therefore, the design constraints referring to the suspension spring and damper are given in Table 2.

Table 2 Co-design constraints for the suspension spring and damper.

$0.0861 \leq D \leq 0.16$	$0.009 \leq d \leq 0.015$	$0.030 \leq p \leq 0.072$
$4d \leq D \leq 12d$	$L_o \leq 5.26D$	$L_o \leq 0.33$
$d + D \leq 0.175$	$D - d \geq 0.071$	$d - D + D_p + 0.022 \leq 0$

The initial values referring to the spring design are selected as the nominal: D_0 = 0.123 m, d_0 = 0.012 m, p_0 = 0.051 m. In relation to the initial values of the damper design, $D_p^0 = 0.03$ m and $L_o^0 = 0.051$ m are assumed, which correspond to the average value of the lower and upper limit of each parameter. These parameters lead to k_s = 17837.08 N/m and b_s = 1510.30 N.s/m, according to Eq. (15), and (16). For comparative analysis between systems, it is assumed that the initial values of the plant design parameters are the same.

Aiming to improve the dynamic behavior of the vehicle considered in this work, the suspension system control project was carried out in order to guarantee both requirements, driving comfort and vehicle safety. In this context, the outputs to be controlled z are the vertical acceleration of the sprung mass ($\ddot{Z}_s$) and the difference between the displacement of the unsprung mass and the irregularity of the track $Z_u - Z_r$. The suspension workspace, $Z_s - Z_u$, was also added as a performance output. The control output y used to feedback the system is the suspension workspace $Z_s - Z_u$. The reason is that this variable corresponds to the extension/compression of the actuator, a quantity that can be measured by the sensors [48].

Based on these considerations, the control matrices for optimizing comfort and safety are given by $A = A_p$, $B_1 = B_r$ and $B_2 = B_A$, as defined in Eq. (12) to (14). The exogenous input w is the disturbance Z_r from road irregularities, and control input u is the active force F_A between sprung and unsprung masses. The output system matrices are given respectively by:

$$\boldsymbol{C_1} = \begin{bmatrix} \frac{-k_s}{m_s} & \frac{-b_s}{m_s} & 0 & 0 \\ 0 & 0 & 1 & 0 \\ 1 & 0 & 0 & 0 \end{bmatrix}; \tag{19}$$

$$\boldsymbol{D_{11}} = \begin{bmatrix} 0 \\ -1 \\ 0 \end{bmatrix}; \boldsymbol{D_{12}} = \begin{bmatrix} \frac{1}{m_s} \\ 0 \\ 0 \end{bmatrix}, \tag{20}$$

$$\boldsymbol{C_2} = \begin{bmatrix} 1 & 0 & 0 & 0 \end{bmatrix}; \boldsymbol{D_{21}} = 0; \boldsymbol{D_{22}} = 0. \tag{21}$$

In the work, functions of the Yalmip Toolbox [26] are used to solve the optimization problems of the controller. The plant optimization was performed using the *fmincon* optimization function. The controller optimization problems were performed using the *sdpt3* solver.

The suspension systems are compared with respect to responses to a given excitation from road irregularities. In this study, two road profiles are defined to excite the suspension system, which are the bump excitation and the sinusoidal excitation.

In this work, the vehicle is considered passing by the bump excitation of 3.70m long and 0.10m high, at a speed of 30*km/h*, as shown in Figure 7(a). For simulations considering the sinusoidal road profile, ω = 8rad/s is defined, which is close to the resonance frequency of the sprung mass. The amplitude of the sine wave is 0.010m, as shown in Figure 7(b).

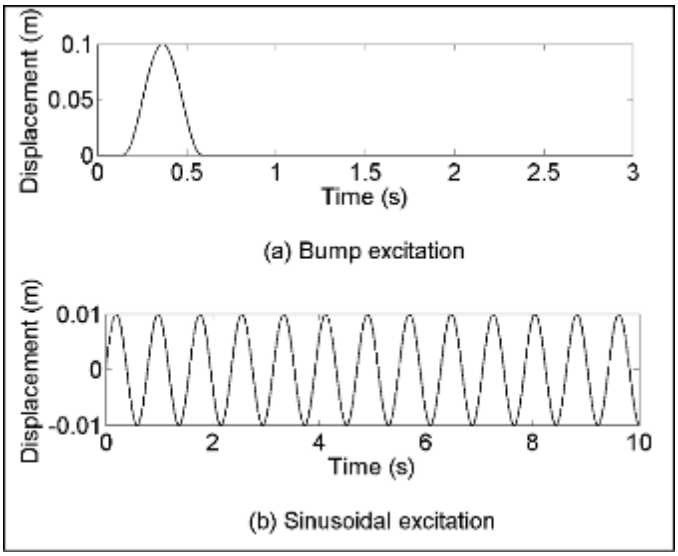

Figure 7 Road profile.

The comparative analysis of the RPO methodology is carried out with the sequential, iterative and nested optimization strategies for the automotive suspension system. The algorithms used for the comparative analysis were presented in [48].

The optimized plant parameters for sequential, iterative nested and RPO are shown in Table 3.

Table 3 Optimized plant design parameters.

	Sequential	**Iterative**	**Nested**	**RPO**
D (m)	0.1226	0.1030	0.0903	0.1380
d (m)	0.0103	0.0097	0.0092	0.0130

p (m)	0.0617	0.0507	0.0561	0.0541
D_p (m)	0.0359	0.0357	0.0334	0.0359
D_o (m)	0.0060	0.0060	0.0052	0.0060
k_s (N/m)	11814.92	11903.61	17514.81	18900.86
b_s (Ns/m)	1243.20	1244.19	1463.82	1252.13

The values of the transfer matrix norms between the exogenous input and the controlled outputs, the magnitude of the spring weights, and the maximum shear stresses in the shock absorber body walls are shown in Table 4, for each of the studied methods. To obtain these results, the weights adopted in Eq. (18) were $H_\infty\% = 0.10$, $\rho\% = 0.30$ and $\tau_{max}\% = 0.60$ for the sequential, iterative and RPO, and $^{H}{}_\infty\% = 0.00$, $\rho\% = 0.40$ and $\tau_{max}\% = 0.60$ for the nested. Maximum values are defined for these parameters in order to normalize Eq. (18), that is, $H_\infty = 1000$, $\varphi = 10\ kg$ and $\tau_{max} = 100\ MPa$.

Table 4 Values of the transfer matrix norms, of the spring weights and the maximum shear stresses in the shock absorber body walls.

Co-design	||Twz(s)||∞	Weight [kg]	τmax [MPa]
Sequential	730.80	1.26	30.15
Iterative	730.87	1.19	30.34
Nested	730.85	0.83	38.58
RPO	730.85	2.55	30.33

It can be seen that the values of the $||T_{wz}(s)||_\infty$ norm are very similar regardless of the optimization strategy employed. The same occurs for the maximum shear, except for the nested method.

Figure 8 shows the behavior of the vertical acceleration of the sprung mass when passing through the bump excitation, as shown in Figure 7(a).

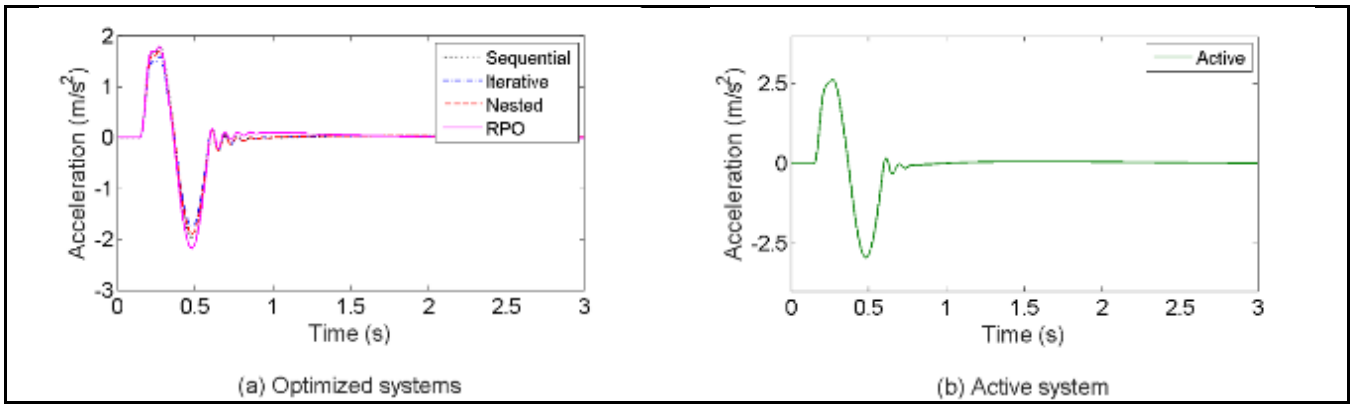

Figure 8 Response of the sprung mass acceleration when passing through the bump excitation.

Table 5 presents the maximum peak, minimum peak, and RMS values of sprung mass vertical acceleration for the studied cases. In addition, the percentage of reduction in relation to the active project is also shown. For the peaks, the reduction obtained in terms of the peak-to-peak value is considered.

Table 5 Optimized plant design parameters – acceleration [m/s²].

	Max. Peak	Min. Peak	RMS	Δ_{peak}[%]	Δ_{RMS}[%]
Sequential	1.313	-1.424	0.374	7.2	7.4
Iterative	0.788	-0.833	0.216	45.0	46.5

Nested	0.867	-0.921	0.240	39.4	40.5
RPO	0.909	-0.969	0.252	36.3	37.6

It can be seen, through Figure 8(a) and Table 5, that the RPO has a performance equivalent to the iterative and nested methods, but with a slight deterioration in relation to the peak value of the temporal response and the RMS value of the sprung mass acceleration. However, the method maintained a substantial improvement over the sequential co-design and the non-optimized active design, as can be seen by comparing Figure 8(a) with Figure 8(b).

Figure 9 shows the behavior of the contact force between the tire and the track when the vehicle is subjected to bump excitation.

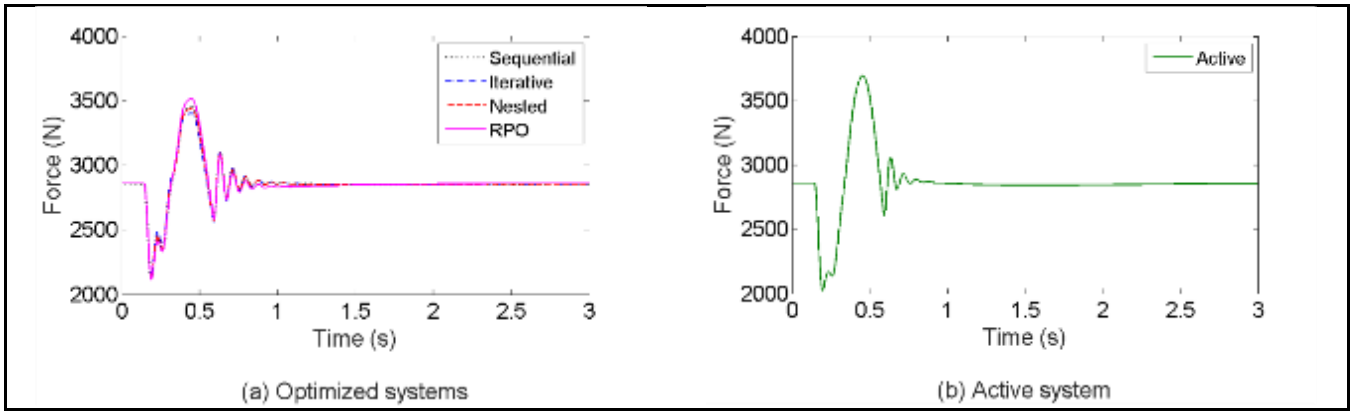

Figure 9 Response of the contact force when passing through the bump excitation**.**

The maximum and minimum peak values of the contact force between the tire and the track for the sequential design, the iterative design, the nested design and the RPO are shown in Table 6. In addition, the reduction percentage of the peak value of the time response of each co-design in relation to the active system is also shown.

Table 6 Optimized plant design parameters - Force [N].

	Max. Peak	**Min. Peak**	**Δ_{peak}[%]**
Sequential	3358.76	2161.91	1.6
Iterative	3350.98	2205.18	5.8
Nested	3347.48	2199.10	5.5
RPO	3346.49	2195.78	5.4

When comparing Figures 9(a) and 9(b), it is verified that the sequential, iterative, nested co-design method and the RPO maintained an improvement in relation to the non-optimized active design.

The behavior of the vertical acceleration of the sprung mass and the contact force between the tire and the track, when passing through the sinusoidal excitation, as illustrated in Figure 7(b), is shown, respectively, in Figures 10 and 11.

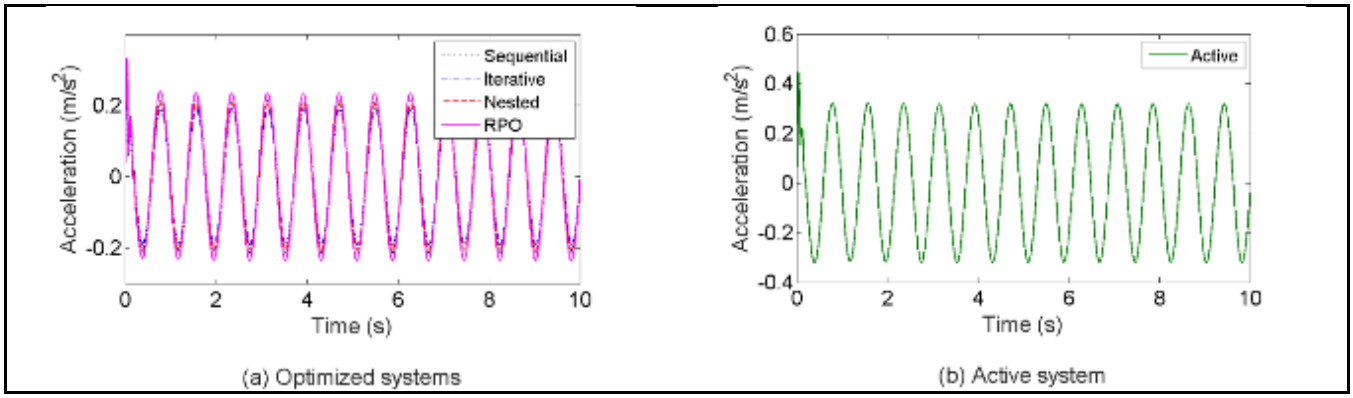

Figure 10 Response of the sprung mass acceleration when passing through the sinusoidal excitation.

Table 7 presents the sprung mass vertical acceleration RMS values for sequential design, iterative design, nested design and RPO. In addition, the reduction of the RMS value of each co-design in relation to the active system is also shown.

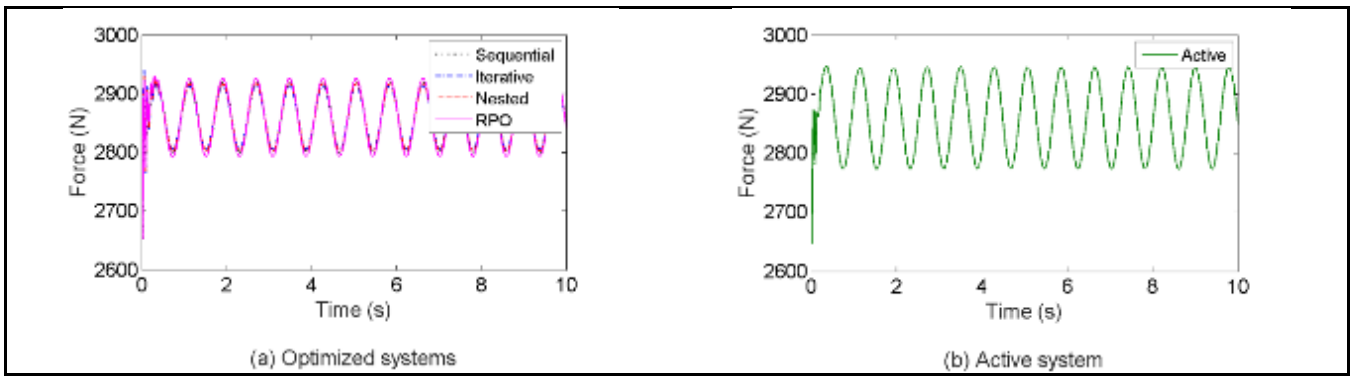

Figure 11 Response of the contact force when passing through the sinusoidal excitation.

Table 7 Optimized plant design parameters - acceleration [m/s²] .

	RMS	**Δ_{RMS}[%]**
Sequential	0.108	7.6
Iterative	0.062	47.0
Nested	0.069	41.0
RPO	0.073	37.6

Comparing the methods with this type of excitation, similar results are found in comparison to the spine case. From Figure 10, it can be seen that the RPO improves the vertical acceleration at the resonant frequency of the sprung mass in relation to the active system.

In relation to vehicle safety, it is observed through Figure 11 that the RPO method presents values for the road contact force that are lower than the active system, contributing to the improvement of vehicle safety. The RPO strategy leads to results far superior to the non-optimized active design, as expected. Both comfort and vehicle safety have been substantially improved.

6. Conclusion

This paper presented a control co-design methodology termed Robust Polytopic Optimization (RPO), applicable to a class of linear dynamical systems subject to parametric uncertainties. The proposed approach integrates plant optimization and controller synthesis within a polytopic robust control framework, enabling a two-level optimization strategy that preserves closed-loop stability throughout the entire co-design process.

At each iteration, a robust controller is synthesized based on a polytopic representation of the plant uncertainties, and subsequently employed in the plant optimization step while maintaining the closed-loop performance specifications. A distinctive feature of the RPO methodology is the progressive reduction of the uncertainty polytope, which systematically alleviates the conservativeness typically associated with robust control-based co-design approaches. This iterative process is repeated until a predefined stopping criterion is satisfied, leading to a consistent and efficient convergence toward an optimized plant–controller pair.

The effectiveness of the proposed methodology was demonstrated through the co-design of an automotive active suspension system, targeting improvements in driving comfort and vehicle safety. In this application, the suspension spring stiffness and damping coefficients were treated as dependent variables governed by geometric constraints, allowing the co-design problem to capture realistic physical relationships between plant parameters. The obtained results indicate that the RPO strategy achieves performance levels comparable to, and in some cases exceeding, those of conventional sequential, iterative, and nested co-design approaches, while ensuring robustness and closed-loop stability at every stage of the optimization.

Although illustrated using an automotive suspension system, the proposed framework is not limited to this specific application and can be extended to other control-oriented and mechatronic design problems involving parametric uncertainties. Future research will focus on extending the RPO methodology to time-varying and nonlinear systems, as well as on its application to broader classes of multidisciplinary engineering design problems.

Compliance with ethical standards

Acknowledgments

This work was supported by the Coordination for the Improvement of Higher Education Personnel – Brazil (CAPES).

Disclosure of conflict of interest

No conflict of interest to be disclosed.

References

[1] C. Wuwei and W. Qirui, Integrated design of structure/control systems of semi–active suspension using genetic algorithms and H_∞ control scheme, Int. J. Vehicle Autonomous Systems **1**, 387 (2003).

[2] R. Patil, Z. Filipi, and H. Fathy, Computationally efficient combined design and control optimization using a coupling measure, in *Proc. of the IFAC Symposium on Mechatronic Systems* (2010) pp. 144–151.

[3] J. Allison, T. Guo, and Z. Han, Co-design of an active suspension using simultaneous dynamic optimization, Journal of Mechanical Design **136**, 1 (2014).

[4] H. Fathy, P. Papalambros, A. Ulsoy, and D. Hrovat, Nested plant/controller optimization with application to combined passive/active automotive suspensions, in *Proc. of the American Control Conference* (2003) pp. 3375–3380.

[5] M. Garcia-Sanz, Control co-design: an engineering game changer, Advanced Control for Applications: Engineering and Industrial Systems **1**, 1 (2019).

[6] H. Fathy, P. Papalambros, and A. Ulsoy, Integrated plant, observer, and controller optimization with application to combined passive/active automotive suspensions, in *Proc. of the Mech. Engineering Congress and Exposition* (2003) pp. 15–21.

[7] W. Chen, Q. Wang, J. Mills, and D. Sun, Integrated design of structure/control systems of semi-active suspension using genetic algorithms and H_∞ control scheme, International Journal Vehicle Autonomous Systems **1**, 387 (2003).

[8] S. Alyaqout, P. Papalambros, and A. Ulsoy, Combined design and robust control of a vehicle passive/active suspension, International Journal Vehicle Design **59**, 315 (2012).

[9] M. Alexander, J. Allison, and P. Papalambros, Decomposition-based design optimization of electric vehicle powertrains using proper orthogonal decomposition, International Journal of Powertrains **1**, 72 (2012).

[10] T. Hofman and N. Jansen, Integrated design optimization of the transmission system and vehicle control for electric vehicles, IFAC–PapersOnLine **50**, 10072 (2017).

[11] S. Azad, M. Behtash, H. A., and M. J. Alexander-Ramos, PHEV powertrain co-design with vehicle performance considerations using MDSDO, Struct. Multidiscip. Optimization **60**, 1155 (2019).

[12] A. K. Sundarrajan and D. R. Herber, Towards a fair comparison between the nested and simultaneous control co-design methods using an active suspension case study, in *American Control Conference* (2021) pp. 1–8.

[13] G. E. Barter, A. Robertson, and W. Musial, A systems engineering vision for floating offshore wind cost optimization, Renewable Energy Focus **34**, 1 (2020).

[14] J. Deese, P. Tkacik, and C. Vermillion, Gaussian process-driven, nested experimental co-design: theoretical framework and application to an airborne wind energy system, Journal of Dynamic Systems, Measurement, and Control **143**, 1 (2020).

[15] J. Jonkman, A. Wright, G. Barter, M. Hall, J. T. Allison, and D. R. Herber, Functional requirements for the weis toolset to enable controls co-design of floating offshore wind turbines, in *Intnl. Offshore Wind Technical Conference* (2021) pp. 1–13.

[16] A. L. Nash and N. Jain, Hierarchical control co-design using a model fidelity-based decomposition framework, J. Mech. Design **143**, 1 (2020).

[17] F. Angelettia, P. Iannellib, and P. Gasbarria, Automated nested co-design framework for structural/control dynamics in flexible space systems, Acta Astronautica **198**, 445 (2020).

[18] K. B. Sanchez-Sanchez and L. A. Ricardez-Sandoval, Simultaneous design and control under uncertainty using model predictive control, Industrial Engineering Chemistry Research **53**, 4815 (2013).

[19] P. V. Chanekar and N. C., Co-design of Lipschitz nonlinear systems, arXiv: 2201.03886, 1 (2022).

[20] S. Azad and D. Herber, An overview of uncertain control co-design formulations, Journal of Mechanical Design **145** (2023).

[21] A. L. Nash, H. C. Pangborn, and N. Jain, Robust control co-design with receding-horizon mpc, in *American Control Conference* (2021) pp. 373–379.

[22] Y.-K. Tsai and R. Malak, Robust control co-design using tube-based model predictive control, in *Proc. of the American Control Conference* (2023) pp. 769–775.

[23] T. J. Bird, J. A. Siefert, H. C. Pangborn, and N. Jain, A set-based approach for robust control co-design, in *Proc. of the 2024 American Control Conference – IEEE* (2024) pp. 2564–2571.

[24] S. Boyd, L. El Ghaoui, E. Feron, and V. Balakrishnan, *Linear matrix inequalities in system and control theory*, 1st ed. (Society for industrial and applied mathematics, Philadelphia, 1994) p. 193.

[25] C. Scherer, P. Gahinet, and M. Chilali, Multiobjective output-feedback control via LMI optimization, IEEE Transactions on Automatic Control **42**, 896 (1997).

[26] J. Löfberg, YALMIP: A toolbox for modeling and optimization in MATLAB, IEEE International Symposium on Computer Aided Control Systems Design **2-4**, 284 (2004).

[27] C. M. Agulhari, A. Felipe, R. C. Oliveira, and P. L. Peres, Algorithm 998: The robust LMI parser—a toolbox to construct LMI conditions for uncertain systems, ACM Transactions on Mathematical Software (TOMS) **45**, 1 (2019).

[28] L. Rodrigues, R. Oliveira, and J. Camino, Parameterized LMIs for robust and state feedback control of continuous-time polytopic systems, International Journal of Robust and Nonlinear Control **28**, 940 (2018).

[29] V. Campos, A.-T. Nguyen, and R. M. Palhares, Adaptive gain-scheduling control for continuous-time systems with polytopic uncertainties: An LMI-based approach, Automatica **133**, 109856 (2021).

[30] R. Franco, H. R´ıos, A. F. de Loza, and D. Efimov, A robust nonlinear model reference adaptive control for disturbed linear systems: An LMI approach, IEEE Transactions on Automatic Control **67**, 1937 (2022).

[31] A. Ladel, A. Benzaouia, R. Outbib, M. Ouladsine, and E. M. El Adel, Robust fault tolerant control of continuous-time switched systems: an LMI approach, Nonlinear Analysis: Hybrid Systems **39**, 100950 (2021).

[32] A. Bisoffi, C. D. Persis, and P. Tesi, Learning controllers for performance through lmi regions, IEEE Transactions on Automatic Control **68**, 4351 (2023).

[33] J. A. Reyer, H. K. Fathy, P. Y. Papalambros, and A. G. Ulsoy, Comparison of combined embodiment design and control optimization strategies using optimality conditions, in *ASME Design Engineering Technical Conference* (2001) pp. 1–10.

[34] J. Onoda and R. T. Haftka, An approach to structure/control simultaneous optimization for large flexible spacecraft, AIAA Journal **25**, 1133 (1987).

[35] W. K. Belvin and K. C. Park, Structural tailoring and feedback control synthesis: an inter-disciplinary approach, AIAA Journal of Guidance, Control, and Dynamics **13**, 424 (1990).

[36] A. P. Deshmukh and J. T. Allison, Multidisciplinary dynamic optimization of horizontal axis wind turbine design, Structural and Multidisciplinary Optimization **53**, 15 (2016).

[37] C. M. Chilan, D. R. Herber, N. Y. K., S.-J. Chung, J. T. Allison, J. B. Aldrich, and O. S. Alvarez-Salazar, Co-design of strain-actuated solar arrays for spacecraft precision pointing and jitter reduction, AIAA Journal **55**, 3180 (2017).

[38] D. Herber, *Dynamic system optimization of wave energy converters utilizing direct transcription*, Master's thesis, University of Illinois at Urbana-Champaign, Urbana, USA (2014).

[39] D. Peters, *Coupling and controllability in optimal design and control*, Ph.D. thesis, University of Michigan, Ann Arbor, USA (2010).

[40] P. Gahinet and P. Apkarian, A linear matrix inequality approach to H_∞ control, International Journal of Robust and Nonlinear Control **4**, 421 (1994).

[41] R. Oliveira, V. Montagner, P. Peres, and P. Bliman, LMI relaxations for H_∞ control of time-varying polytopic systems by means of parameter-dependent quadratically stabilizing gains, IFAC Proceedings Volumes **40**, 614 (2007).

[42] H. Taguitad and E. Esmailzadeh, Automobile passenger comfort assured through LQG/LQR active suspension, Journal of Vibration and Control **4**, 603 (1998).

[43] I. Martins, J. Esteves, G. Marques, and F. Pina da Silva, Permanent-magnets linear actuators applicability in automobile active suspension, IEEE Transactions on Vehicular Technology **55**, 86 (2006).

[44] R. Budynas and K. Nisbett, *Shigley's Mechanical engineering design*, 9th ed. (McGraw-Hill, New York, 2018) p. 1120.

[45] R. Hibbeler, *Mechanics of Materials*, 10th ed. (Pearson, London, 2018) p. 896.

[46] L. Pereira, *Analysis of the experimental survey methodology to obtain the suspension parameters of a vehicle (in portuguese)*, Undergraduate Thesis, Federal University of Pará, Belém, Brazil (2011).

[47] J. Reimpell, H. Stoll, and J. Betzler, *The automotive chassis: engineering principles*, 2nd ed. (Elsevier, Oxford, 2001) p. 460.

[48] S. Dutra, *Co-design of vehicle active suspension systems (in portuguese)*, Master's thesis, Federal University of Santa Catarina, Joinville, Brazil (2019).